

The Role of H^+/OH^- Channels in the Salt Stress Response of *Chara australis*

Mary J. Beilby · Sabah Al Khazaaly

Received: 9 April 2009 / Accepted: 2 June 2009 / Published online: 17 July 2009
© Springer Science+Business Media, LLC 2009

Abstract We investigate the electrophysiological salt stress response of the salt-sensitive charophyte *Chara australis* as a function of time in saline artificial pond water (saline APW) containing 50 mM NaCl and 0.1 mM CaCl₂. The effects are due to an increase in Na⁺ concentration rather than an increase in Cl⁻ concentration or medium osmolarity. A previous paper (Shepherd et al. Plant Cell Environ 31:1575–1591, 2008) described the rise in the background conductance and inhibition of proton pumping in saline APW in the first 60 min. Here we investigate the shift of membrane potential difference (PD) to levels above –100 mV and the change of shape of the current–voltage (I/V) profiles to upwardly concave. Arguing from thermodynamics, the I/V characteristics can be modeled by channels that conduct H⁺ or OH⁻. OH⁻ was chosen, as H⁺ required an unrealistic increase in the number/permeability of the channels at higher pH levels. Prolonged exposure to saline APW stimulated opening of more OH⁻ channels. Recovery was still possible even at a PD near –50 mV, with partial return of proton pumping and a decrease in OH⁻ current following APW wash. Upon change of pH from 7 to 9, the response was consistent with previously observed I/V characteristics of OH⁻ channels. For a pH change to 6, the response was transient before channel closure but could still be modeled. The consequences of opening of H⁺ or OH⁻ channels while the cell is under salt stress are discussed.

Keywords Salt stress · Charophytes H⁺/OH⁻ channels · Current–voltage analysis

The experiments described in this paper are a part of a larger investigation that compares the electrophysiology of salt-sensitive and salt-tolerant charophytes challenged by saline stress. To gain a full understanding of the ability of salt-tolerant plants to survive in saline media, it is also necessary to study the pathology of salt stress in their salt-sensitive relatives. The salt-tolerant charophyte *Lamprothamnium* thrives in brackish coastal lakes where salinity can be higher than that of seawater at the time of drought (Shepherd et al. 1999). The salt-sensitive *Chara australis* dies within 6 days in media with 50 mM NaCl and 0.1 mM Ca²⁺. Thus comparing the electrophysiological responses to salinity of these closely related plants of ancient lineage is likely to identify a minimal ensemble of factors that influence salt tolerance (Tester and Davenport 2003).

In plant cells proton ATPase at the plasma membrane pumps protons out of the cytoplasm. The resulting negative membrane potential difference (PD) energizes the import of nutrients and export of undesirable ions, such as Na⁺. The proton pump in *Lamprothamnium* is stimulated by both a decrease in internal pressure (increase in medium osmolarity) and an increase in medium salinity (Al Khazaaly and Beilby 2007). The proton pump in *Chara australis*, on the other hand, is insensitive to a decrease in internal pressure and becomes inhibited by salinity, especially if the calcium ion in the medium is low. In a previous paper we modeled the decline of the proton pump toward the passive background state with a resting PD near –100 mV and documented an increase in the background conductance and onset of repetitive spontaneous action potentials (APs) in the first 60 min of salinity stress (Shepherd et al. 2008).

M. J. Beilby (✉) · S. Al Khazaaly
Department of Biophysics, School of Physics, The University of
New South Wales, Sydney, NSW 2052, Australia
e-mail: mjb@newt.phys.unsw.edu.au

In this paper we follow further development of electrical characteristics of *Chara* cells after longer exposure to salinity stress. Cells were pretreated with sorbitol APW (artificial pond water). The I/V characteristics were pump current-dominated (see Fig. 1a, open squares, and Fig. 1c and d, heavy solid lines). After exposure to saline APW of the same osmolarity the membrane PD moved toward -100 mV and the shape of the I/V profile transformed close to linear—the background state (Fig. 1a, triangles, and Fig. 1c and d, short-dashed lines). In this case there is still a low pump current component present. With further exposure to saline APW the I/V characteristics became upwardly concave (Fig. 1a, diamonds, and Fig. 1c and d, long-dashed lines). Such I/V characteristics suggest the contribution of a negative current (outflow of negative charge or inflow of positive charge) with a reversal PD at 0

or positive PDs. The ions with the appropriate inside and outside concentrations are Cl^- , Ca^{2+} , and proton (H^+) or hydroxyl (OH^-). Large currents of Ca^{2+} are unlikely and would result in stoppage of cytoplasmic streaming (Kamimura 1959), which was not observed. Cl^- was eliminated, as replacement of $NaCl$ by Na_2SO_4 in the saline APW did not shift the reversal PD or change the shape of the I/V characteristics. The change of medium pH shifted the membrane PD in the right direction and affected the shape of the I/V characteristics. Consequently, we modeled the negative current as inflow of H^+ or outflow of OH^- , employing the Goldman-Hodgkin-Katz (GHK) equation.

The H^+ / OH^- channels are well documented in charophytes. The discovery of acid and alkaline bands along the surface of charophyte cells (Spear et al. 1969; Lucas and Smith 1973) was one of the starting points for research into

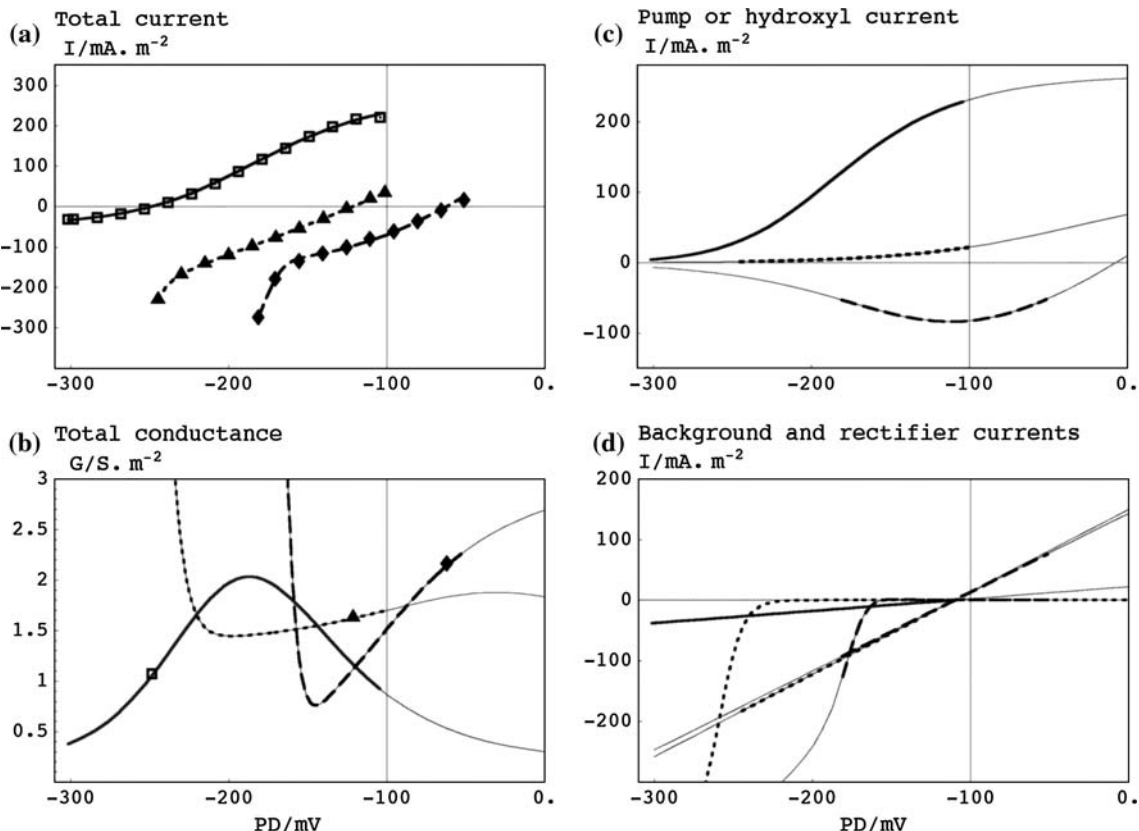


Fig. 1 **a** A typical trend in the I/V characteristics from the pump-dominated profile (empty rectangles) in sorbitol APW to the background current-dominated profile after 67 min of saline APW (filled triangles). After 117 min of saline APW the membrane PD depolarized further and the profile exhibited an upward bend (filled diamonds). Experimental data are simulated by background current and pump (solid line; model parameters—background current $g_{bkg} = 0.2 \text{ S m}^{-2}$, $V_{bkg} = -110 \text{ mV}$; pump parameters— $k_{io}^0 = 7200 \text{ s}^{-1}$, $k_{oi}^0 = 2.9 \text{ s}^{-1}$, $\kappa_{io} = 0.5 \text{ s}^{-1}$, $\kappa_{oi} = 138 \text{ s}^{-1}$); by background current, declining pump, and inward rectifier current (short-dashed line; model parameters—background current $g_{bkg} = 1.36 \text{ S m}^{-2}$, $V_{bkg} = -110 \text{ mV}$; pump parameters— $k_{io}^0 = 100 \text{ s}^{-1}$,

$k_{oi}^0 = 0.1 \text{ s}^{-1}$, $\kappa_{io} = 0.5 \text{ s}^{-1}$, $\kappa_{oi} = 55 \text{ s}^{-1}$; inward rectifier parameters— $N_K P_K = 40 \times 10^{-7} \text{ m s}^{-1}$, $V_{50} = -258 \text{ mV}$, $z_g = 3.5$); and by background current, OH^- channels, and inward rectifier current (long-dashed line; model parameters—background current $g_{bkg} = 1.3 \text{ S m}^{-2}$, $V_{bkg} = -110 \text{ mV}$; OH^- channel parameters— $N_{OH} P_{OH} = 35 \times 10^{-4} \text{ m s}^{-1}$, $V_{50-} = -130 \text{ mV}$, $z_{g-} = 0.6$; inward rectifier parameters— $N_K P_K = 40 \times 10^{-7} \text{ m s}^{-1}$, $V_{50} = -174 \text{ mV}$, $z_g = 4$, $pH_i = 6.98$). **b** Total conductance-voltage profiles, with the resting PD indicated on each curve by a point of the same type as in a. **c** Pump currents and OH^- current. **d** Background currents and inward rectifier currents. The thin solid lines in **b-d** show extrapolation of the models beyond the PD window delimited by the data

the localized transporter operation and external currents flowing between these specialized cell zones (Walker and Smith 1977; Lucas and Nuccitelli 1980). The transporter active in the acid zone is the proton pump creating the H^+ efflux, while the alkaline zones facilitate opening of channels conducting H^+ or OH^- (Bisson and Walker 1980; Lucas 1982). While it is clear that the banding system helps cells assimilate carbon, different schemes have been proposed involving CO_2 or HCO_3^- transport (Walker et al. 1980; Lucas 1982).

Speculation about whether the channels conduct H^+ or OH^- has remained unresolved for almost 40 years. OH^- is the favored ion, as the concentration of H^+ is very low in the alkaline bands, where the pH rises up to 10.5. Bisson and Walker (1980), Smith and Walker (1983), and Beilby and Bisson (1992) measured conductances of up to 10 S/m^2 , which would be difficult to sustain with so few H^+ ions in the vicinity of the membrane, unless there is water splitting in the membrane due to high electric fields (Simons 1979). Lucas (1979) also argued for OH^- to be the transported ion. However, the definitive experiment is yet to be designed and so we continue to refer to the channels as H^+/OH^- .

Under normal nonsaline conditions *Chara* H^+/OH^- channels are activated at a high external pH, ≥ 9.0 (Bisson and Walker 1980). It is not yet known why saline APW opens the H^+/OH^- channels at a neutral medium pH. However, this new aspect of salinity stress contributes to cell deterioration, as the proton electrochemical gradient is dissipated and the cytoplasm becomes more acid.

Extant Charales are a sister group to the ancestors of all land plants (Karol et al. 2001) and their cellular responses to salinity are likely to reveal fundamental mechanisms with wider applications. Acid and alkaline zones were found in aquatic angiosperms (Prins et al. 1980). Raven (1991) surveyed rhizophytes from many habitats, exhibiting H^+ (or OH^-) currents in root tips that assist with nutrient acquisition. The similarity between salt-sensitive charophytes and roots of crops is discussed.

Materials and Methods

Cell Culture

Chara australis Brown (Garcia and Chivas 2006) was collected from a golf course lake at Little Bay, Sydney, and planted in round containers on a bed of autoclaved garden soil, covered with rainwater, with a handful of rotting leaves added. *C. australis* was cultured under equal numbers of Sylvania Gro-Lux fluorescent tubes (Sylvania Australasia, Pty. Ltd.) and cool white fluorescent tubes, providing photosynthetically active radiation of $80\text{ }\mu\text{mol m}^{-2}\text{ s}^{-1}$, on a cycle of 10 h light and 14 h

darkness. Young subapical internodal cells, 7–15 mm long and between 0.6 and 0.7 mm in diameter, were trimmed from healthy plants and left to recover in artificial pond water (APW) for at least 3 days. Experiments were conducted at room temperature (25°C).

Electrophysiology

The internal microelectrode was placed in the large vacuolar compartment. Thus the PD was measured across both the plasma membrane and the tonoplast. However, the plasma membrane I/V characteristics dominate under most conditions because of the high tonoplast conductance (Beilby 1990). Cells were placed in a three-compartment holder, with each compartment insulated by grease. The voltage-clamp was achieved by passing current between Ag/AgCl wire electrodes in the outside and middle compartments (Beilby 1989; Beilby and Shepherd 1996). We measured current-voltage (I/V) characteristics using a bipolar staircase voltage command, with pulses of width between 60 and 100 ms, separated by 120–250 ms, at the resting PD. The data-logging rate was one measurement per millisecond (Beilby and Beilby 1983). The resting PD was data-logged separately at a rate of one PD measurement every 10 s in early experiments and at 10 points per second in later experiments.

Experimental Protocol and Media

In the experimental protocol the cells were inserted into the apparatus and left to recover in the APW for about 1 h. Sorbitol APW was then introduced into the chamber for another hour. I/V characteristics were monitored in both APW and sorbitol APW. Finally, sorbitol APW was exchanged for saline APW and a series of I/V characteristics was recorded. Thus the effects measured were due to salinity stress, as distinct from a decrease in turgor. Some cells were returned to APW and the electrophysiology of the recovery was recorded. To maintain the composition constant the bathing medium was often refreshed by hand. The pH changes of the saline APW were performed quickly, as the electrophysiology of the cells was changing slowly as a function of time in saline APW.

APW consisted of (mM) 0.1 KCl, 1.0 NaCl, 0.1 $CaCl_2$, 2.0 HEPES [4-(2-hydroxyethyl)-1-piperazineethanesulfonic acid], pH 7. Sorbitol APW was made from APW by adding 90 mM sorbitol to match the osmolarity of saline APW. Saline APW was made from APW by adding 50 mM NaCl. For saline APW of pH 9, HEPES was replaced with AMPSO [N -(1,1-dimethyl-2-hydroxyethyl)-3-amino-2-hydroxypropanesulfonic acid] at the same concentration. For saline APW of pH 6, the buffer was MES [2-(*N*-morpholino)ethanesulfonic acid]. The buffer concentration was increased to 5.0 mM in saline APW.

Modeling

The total clamp current was resolved into contributions made by parallel populations of ion transporters. The proton pump current I_p was modeled by the two-state Hansen et al. (1981) model. This model has been used extensively to model chloride or proton ATPases in *Acetabularia*, charophytes, guard cells, and wheat root protoplasts (Gradmann 1989; Beilby 1984; Blatt 1987; Tyerman et al. 2001).

$$I_p = z_p FN \frac{k_{io}\kappa_{oi} - k_{oi}\kappa_{io}}{k_{io} + k_{oi} + \kappa_{io} + \kappa_{oi}} \quad (1)$$

$$k_{io} = k_{oi}^o e^{\frac{zFV}{2RT}} \quad (2)$$

$$k_{oi} = k_{oi}^o e^{-\frac{zFV}{2RT}} \quad (3)$$

where F , R , and T have their usual meanings, and z_p is the pump stoichiometry, which has been set to 1. N is a scaling factor (2×10^{-8}) and V is the PD across the membrane(s). The number of carrier states was reduced to two with a pair of PD-dependent constants, k_{io} and k_{oi} , with a symmetric Eyring barrier and two PD-independent rate constants, κ_{io} and κ_{oi} . These constants are fitted to the data.

The background current was fitted by an empirical equation:

$$I_{bkg} = g_{bkg} (V - V_{bkg}) \quad (4)$$

The channels passing I_{bkg} are thought to be the equivalent of nonselective cation-permeable channels (NCCs) found in land plants (Shepherd et al. 2002; Demidchik and Maathuis 2007; Demidchik et al. 2002). The reasons for choosing this form of the background current are explained in the Discussion.

The inward and outward rectifiers (with K^+ as the permeant ion) and H^+/OH^- channels were fitted by the GHK equation, with the channel number/permeability as the single parameter (Eq. 5). The moderate PD dependence of the GHK model was supplemented by multiplying by the Boltzmann distribution of open probabilities P_{o-} (Eq. 6) for the inward rectifier, I_{irc} , P_{o+} (Eq. 7) for the outward rectifier, I_{orc} , and both probabilities for the OH^- current, I_{OH} .

$$I_X = P_{o+}P_{o-} \left[\frac{N_X P_X (zF)^2 V ([X]_i - [X]_o e^{-\frac{zFV}{RT}})}{RT (1 - e^{-\frac{zFV}{RT}})} \right] \quad (5)$$

$$P_{o-} = 1 - \frac{1}{1 + e^{-\frac{zgF(V-V_{50})}{RT}}} \quad (6)$$

$$P_{o+} = \frac{1}{1 + e^{-\frac{zgF(V-V_{50})}{RT}}} \quad (7)$$

where z is the valence of the transported ion, and $[X]_o$ and $[X]_i$ are the ion concentrations in the medium and in the cytoplasm, respectively. $N_X P_X$ stands for the number of X ion channels and their permeability treated as a single

parameter; z_g is the number of gating charges, and V_{50-} and V_{50+} are the half activation potentials, V_{50} , at the negative and positive PDs of channel closure (Amtmann and Sanders 1999; Beilby and Shepherd, 2001).

I/V profiles were fitted by eye. Due to the large number of parameters, a good fit could be achieved with several parameter combinations. Some parameters were constrained by additional information, as outlined in the Discussion. Families of I/V profiles were fitted with minimal parameter changes. The main goal was to visualize the components of the total clamp current and their evolution as a function of exposure to salinity. Conductance-voltage (G/V) characteristics were calculated by differentiating the modeled I/V profiles. G/V profiles sometimes aid interpretation, as parallel conductances of channel and pump populations are directly additive.

Results

Membrane PD and I/V Characteristics as a Function of Time in Saline APW

More than 50 cells were exposed to APW, sorbitol APW, and then saline APW at neutral pH. The membrane PD depolarized in all cells in saline APW, whether they were subjected to repeated voltage-clamping protocol to obtain I/V characteristics or the membrane PD was allowed to vary spontaneously while the salinity noise was measured (Al Khazaaly et al. 2009). However, the time course of the depolarization varied from cell to cell. This effect manifested as large scatter in the statistics for four voltage-clamped cells after 1 h in saline APW (Shepherd et al. 2008). The complexity of the response to low- Ca^{2+} saline APW is due to several mechanisms activated (or inactivated) by salinity: (i) increased background conductance, (ii) salinity-induced noise, (iii) pump inhibition, (iv) activation of negative currents, (v) spontaneous and prolonged action potentials, and (vi) activation of the outward rectifier current. In this paper we investigate mechanism iv in more detail.

Twelve cells were subjected to I/V analysis as a function of time in saline APW. All exhibited depolarization of the membrane PD to levels above -100 mV and upwardly concave I/V characteristics. The pH of the medium was changed in four of these cells. Another four cells were tested for changes of NaCl to Na_2SO_4 : neither membrane PD nor I/V characteristics were affected by this change (results not shown). Thus we could eliminate chloride as a possible carrier of the depolarizing negative currents.

A typical change from the pump-dominated I/V characteristics (open rectangles) in sorbitol APW to the background current-dominated I/V profile after 67 min of saline

APW (filled triangles) and to the upwardly concave I/V characteristics after 117 min of saline APW (diamonds) is shown in Fig. 1a. The pump-dominated I/V characteristics are curved and the resting PD can be more negative than -200 mV. The G/V profile exhibits a maximum near -200 mV, attributed to the proton pump. In the background current-dominated state, the I/V profile is close to linear. Note also the increase in the background conductance in saline APW (Fig. 1d). After 117 min of saline APW the membrane PD depolarized further and the profile exhibited an upward bend (filled diamonds). The modeled components of each I/V profile and the fit parameters are listed in the caption to Fig. 1. The total conductance-voltage profiles are shown in Fig. 1b. The resting conductance (shown in Fig. 1b by symbols on each curve) increased with the time in saline APW.

Development of the H^+/OH^- state with time in saline APW is documented in Fig. 2. At the beginning of this experiment the cell was left to recover from handling and microelectrode insertion for more than an hour in APW and then exposed to sorbitol APW for more than an hour (not shown). I/V characteristics were measured several times. An I/V profile in sorbitol APW that is typical for this cell is shown as black points in Fig. 2b. Figure 2a shows the membrane PD response after the cell was exposed to saline APW (thin vertical line). The membrane PD exhibited a fast shift to -120 mV, followed by a slower trend to levels more positive than -100 mV. I/V scans were performed at 21 min (violet line), 60 min (light-green line), 66 min (blue line), and 74 min (pink line) after the saline APW challenge. The membrane PD moved to -50 mV after the last I/V scan. In a preliminary recovery experiment saline APW was replaced with APW. The sorbitol APW step was omitted to save time and to return the cell to full turgor. To our surprise, the membrane PD returned rapidly to -100 mV and gradually became more negative. I/V characteristics after 33 min of APW (orange line) were recorded.

I/V characteristics in sorbitol APW were fitted by the pump model (Fig. 2d), the background current, and the inward rectifier models (Fig. 2e). I/V characteristics in saline APW were modeled by the background current, the inward rectifier (Fig. 2e), and the OH^- channels (Fig. 2d). The recovery I/V characteristics in APW required both the OH^- channel and pump model (Fig. 2d) and the background current and inward rectifier models (Fig. 2e). The fit parameters are listed in Table 1.

Response to pH Change of Saline APW

To test if H^+/OH^- channels indeed participate in salinity stress, we exposed four cells (cells 5–8) to the same sequence of APW, sorbitol APW, and saline APW. When

the cells exhibited upwardly concave I/V characteristics that we consider typical of H^+/OH^- channels (see Figs. 1a and 2b), the pH of the saline APW was changed to either more alkaline or more acidic values.

Figure 3a shows the membrane PD of cell 5, which was exposed to saline APW (pH 7) for 106 min. The medium pH was increased to 9. The cell responded with two action potentials (APs) and a prompt negative shift of the membrane PD of about 20 mV. Better fits of the data were obtained when the pH_i was increased, especially for the second I/V curve, after about 5 min in alkaline saline APW (see Table 2). For the hydroxyl to flow into the cell, E_{OH} has to be negative of V_{bkg} . In this case both reversal PDs were close. As the resting PD settled close to -90 mV, we set V_{bkg} as -90 mV in alkaline saline APW. To fit the hydroxyl current at pH 9, the $N_{OH}P_{OH}$ parameter decreased slightly. The current started to inactivate at PDs positive of E_{OH} , but no inactivation was seen at negative PDs (see Table 2 for parameters). To obtain an equivalent fit of the data at pH 9 using H^+ channels, the parameter $N_{H}P_{H}$ had to be increased to 1400 m/s. Such a large increase seemed unrealistic and all the data were modeled with OH^- channels. The cells were excitable at this stage of saline stress (Shepherd et al. 2008) and thus APs are often observed upon change of media or after the I/V protocol. The I/V data were discarded if an AP occurred at the time of the I/V scan.

A change from neutral to low pH elicited a positive-going transient in the resting PD. Figure 4a shows the resting PD of cell 7 upon change from pH 9 to pH 6 (see also Table 3). This larger change in pH caused a larger transient, and I/V scans could be performed before the membrane PD repolarized. The cell was exposed to neutral-pH saline APW for 191 min. Upon exposure to pH 9, the membrane PD shifted in a negative direction in a similar fashion to cell 5 (Fig. 3a). The shape of the I/V curves was also similar (Fig. 4b). A change to pH 6 resulted in a positive-going transient of about 76 mV. The I/V scan was run 100 s after the pH decrease. The membrane was left clamped and another I/V scan was run over a greater PD range (see Fig. 4b). Once the membrane PD was free, it continued to move back to negative levels. Another I/V scan was performed. The modeling confirmed that the low pH was closing the hydroxyl channels, and the last I/V curve at pH 6 was fitted by the background current and rectifiers only. The closure of hydroxyl channels caused the membrane PD to tend to V_{bkg} . The PD level at pH 6 approached -88 mV.

Figure 5 shows statistics of the response to pH change for cells 5–8 (see also Table 4). The I/V scans at low pH were done as soon as possible after medium change. The average immediate negative step upon increasing the pH from 7 to 9 was 27 mV (five changes in four cells), with a

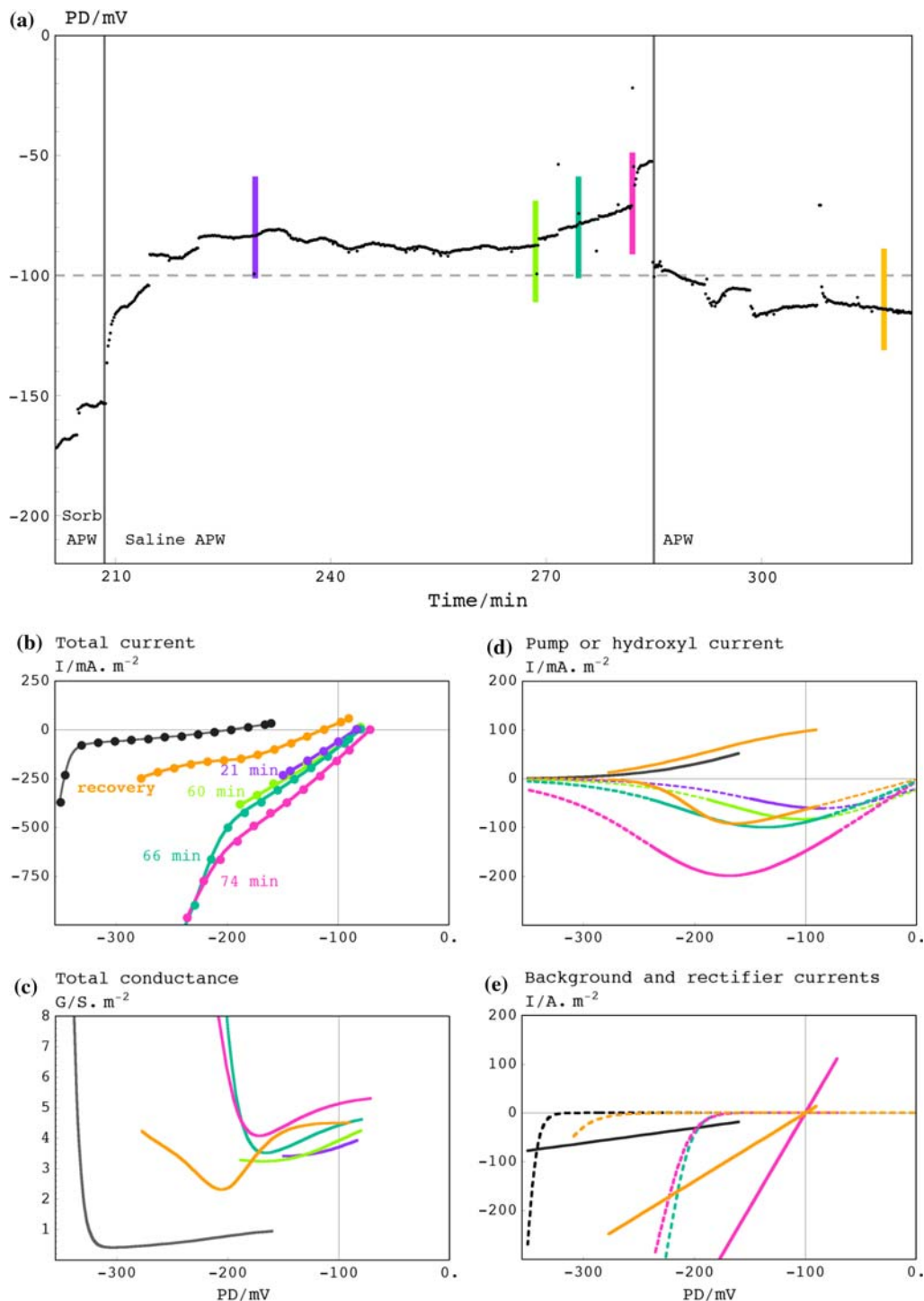


Fig. 2 **a** Response of the membrane PD to salinity. Cell 2 was pretreated in APW for 90 min and in sorbitol APW for 118 min (not shown). The exposure to saline APW is indicated by a vertical line extending across the whole PD range. The membrane shifted to PD levels more positive than -100 mV and the I/V profiles were measured at 21 min (violet), 60 min (light green), 66 min (turquoise), and 74 min (pink) in saline APW. The cell was then returned to APW and the I/V profile was measured at 33 min (orange). The membrane PD was data-logged at 1 point/10 s. **b** The I/V profile in sorbitol APW is depicted by black points and the I/V profiles in saline APW are in colors

corresponding to those in a. Lines represent the total fitted current. **c** The total conductance was calculated by differentiating the current with respect to the membrane PD. **d** The modeled OH^- currents. In this figure, only the modeled OH^- currents were extrapolated beyond the PD window delimited by the data and this is depicted by dashed lines. **e** The fitted background and inward rectifier currents (dashed lines). The background current was fitted as remaining constant in saline APW, thus only the last (pink) line is visible. The parameters of the fit are given in Table 1

Table 1 Fit parameters for modeled currents as a function of time in saline APW (see Fig. 2 and Eqs. 2–5)

Time in medium	I _{OH}		I _{irc}			pH _i	g _{bkg} (S m ⁻²)	E _{OH} (mV)	Resting PD (mV)	
	N _{OH} P _{OH} ($\times 10^{-4}$ m s ⁻¹)	V ₅₀₋ (mV)	z _{g-}	N _K P _K ($\times 10^{-7}$ m s ⁻¹)	V ₅₀ (mV)					
Saline APW										
21 min	25	−200	0.6			6.86	3.1	−8	−83	
60 min	27	−250	0.6			6.825	3.1	−10	−83	
66 min	49	−280	0.6	75	−227	1.8	6.72	3.1	−17	−77
74 min	86	−275	0.6	54	−228	1.8	6.7	3.1	−18	−68
APW wash										
33 min	36	−200	1.5	54	−350	1.45	6.65	1.4	−21	−115

Note: The steady-state I/V profile in sorbitol APW contains a pump component with rate constants $k_{io}^0 = 1000$, $k_{oi}^0 = 0.1$, $\kappa_{io} = 0.5$, and $\kappa_{oi} = 70$ s^{−1} (see Eq. 1); an inward rectifier with $N_KP_K = 54 \times 10^{-7}$ m s^{−1}, $V_{50} = −352.5$ mV, and $z_g = 5.0$; and background conductance $g_{bkg} = 0.31$ S m^{−2}. Membrane resting PD was −198 mV. V_{bkg} was fitted at −100 mV throughout all the records in sorbitol APW, saline APW, and APW wash. The pump component in APW wash was fitted with $k_{io}^0 = 2100$ s^{−1}, $k_{oi}^0 = 0.1$ s^{−1}, $\kappa_{io} = 0.5$ s^{−1}, and $\kappa_{oi} = 57$ s^{−1}

large range, from 8 to 53 mV. A repeated increase in cell 4 produced a negative-going change of 27 mV upon the first exposure but only 8 mV upon the second exposure. The change from pH 9 to pH 6 produced an average positive-going transient of 59 mV (three changes in three cells), with a range of 43 to 76 mV.

Discussion

Modeling Strategies and Insights

The Background State

Figures 1 and 2 show that salinity stress is yet another condition that induces *Chara* cells to enter, in this case transiently, the “background state.” This state is characterized by near-linear I/V characteristics in the PD window delimited by inward and outward rectifiers, I_{irc} and I_{orc} , which are modeled as separate transporter populations mainly permeable to K^+ . The reversal PD for background current, V_{bkg} , is −100 mV (± 30 mV). There is an abundance of experimental data indicating that the background state underpins all the other PD states. Proton pump inhibition by different types of inhibitors (DES, Azide, Vanadate) and withdrawal of ATP in perfused cells yields very similar background states in *Chara australis* and *longifolia* (Beilby 1984; Yao et al. 1992; Beilby and Walker 1996). Closure of the high-conductance K^+ channels by a blocker such as TEA, Ba^{2+} , Na^+ , or Cs^+ , a high concentration of Ca^{2+} , or a low concentration of K^+ again reveals similar background states (Beilby 1985, 1986a, b; Tester 1988a, b). Cells of the salt-tolerant charophyte *Lamprothamnium* are often found in the background state (Beilby and Shepherd 1996). Comparison of I/V characteristics of

Lamprothamnium cells acclimated to a range of salinities revealed that the background conductance increases with salinity, but the reversal PD remains near −100 mV (Beilby and Shepherd 2001). A similar increase in conductance is found in *Chara* (Beilby and Shepherd 2006; Shepherd et al. 2008) (Figs. 1 and 2). We are assuming that the background current flows through nonselective channels (Demidchik and Mathuis 2007) and that these channels are the main pathways for Na^+ into the cell. While the nonzero reversal PD, which seems relatively insensitive to changes in most ionic concentrations, is yet to be explained, the background currents are well documented not only in charophytes but also in many land plant cells. For instance, a bimodal distribution of membrane PDs and I/V characteristics is observed in guard cells (Thiel et al. 1992). In wheat root protoplasts, linear background currents with nonzero reversal PDs had to be included to match the measured proton fluxes with the measured total currents (Tyerman et al. 2001).

Modeling H^+/OH^- Channels

The early I/V characteristics in saline APW (violet and green I/V curves; Fig. 2b) exhibit reversal PDs only slightly positive with respect to −100 mV (reversal PD for the background current). The profiles are nearly linear, with only a hint of curvature, as the contribution of the negative current is small. However, with time in saline APW, the membrane PD becomes less negative and the upwardly concave shape more pronounced (blue and pink I/V curves; Fig. 2b). We model this development by increasing the combined parameter for hydroxyl channel number and permeability, $N_{OH}P_{OH}$ (see Fig. 2d and Table 1). The upwardly concave shape arises from the PD dependence of the hydroxyl current. The current decreases

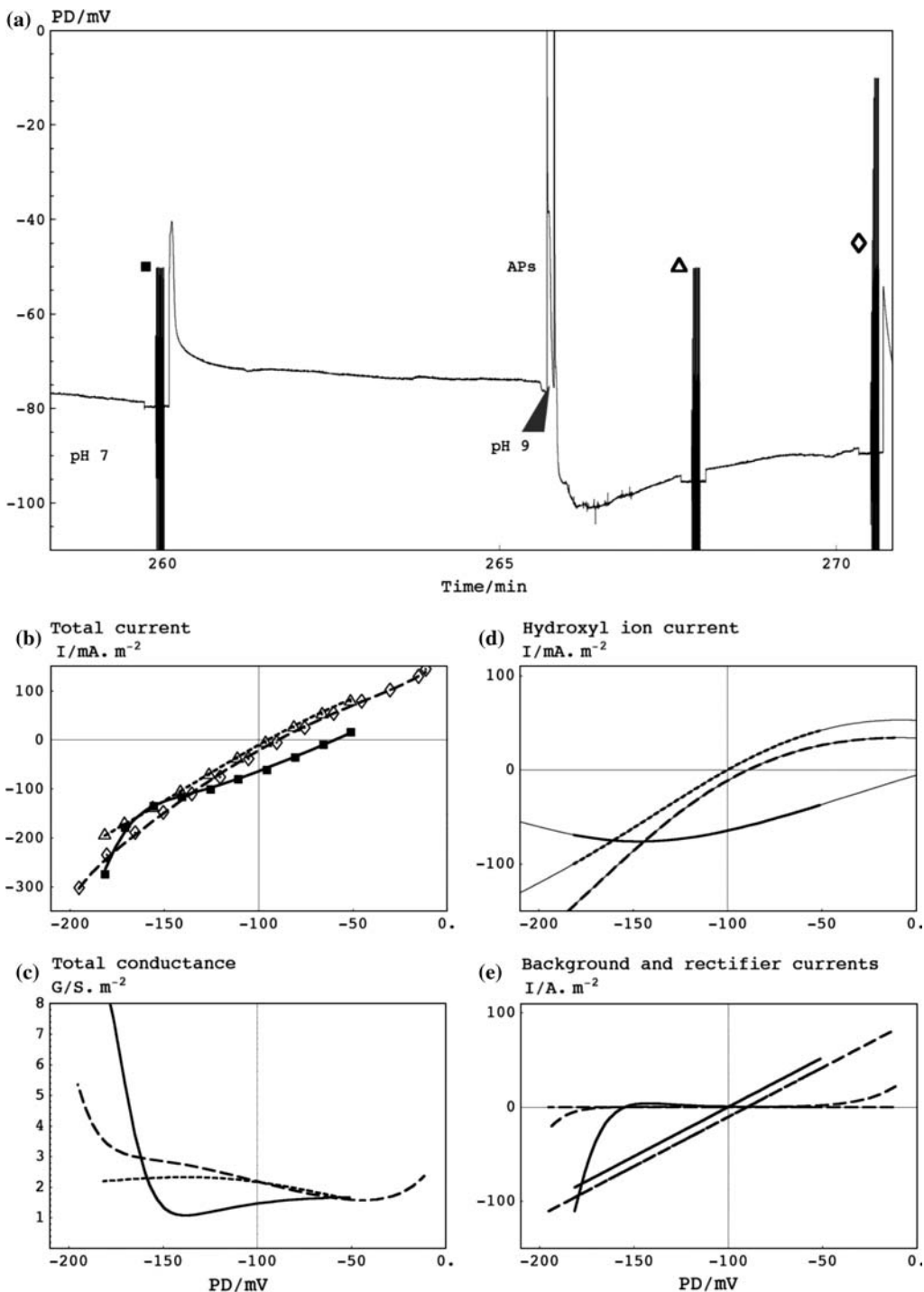


Fig. 3 **a** Response of the membrane PD in saline APW to a change in pH from 7 to 9 (cell 5). The membrane PD was data-logged at the faster rate of 10 points/s. The horizontal axis shows the time from the start of the experiment, with the cell exposed to saline APW at 152 min. At this data-logging speed and the scale of the time axis, the I/V staircases appear as thick vertical bars. These are designated by different symbols (full square, open triangle, and open diamond). The change to pH 9 is indicated by an arrow. Action potentials can be seen after the first and third I/V data collection and upon change of saline

APW. **b** The I/V profiles are shown as points using the same symbols as in a. The data are modeled (solid line for pH 7, short-dashed line for the first I/V curve at pH 9, long-dashed line for the second I/V curve at pH 9). The modeling parameters are given in Table 2. **c** G/V profiles are obtained by differentiation of the I/V profiles. **d** OH^- currents. The thin solid lines show extrapolation of the model beyond the PD window delimited by the data. **e** Background and rectifier currents. The background current was fitted as remaining constant at pH 9. The same types of lines are used in b-e

Table 2 Parameters for modeled currents to fit data from saline APW of pH 7 and 9 (see Fig. 3 and Eqs. 2–5)

pH _o	I _{OH}	I _{irc}					I _{orc}			pH _i	g _{bkg} (S m ⁻²)	E _{OH} (mV)	Resting PD (mV)
		N _{OH} P _{OH} ($\times 10^{-4}$ m s ⁻¹)	V ₅₀₋	z _{g-}	V ₅₀₊	z _{g+}	N _K P _K ($\times 10^{-7}$ m s ⁻¹)	V ₅₀ (mV)	z _g				
7	11	–185	0.6		50		–181	2.5		7.25	1.05	9	–60
9	9		–117	0.6						7.32	1.05	–100	–95
9	9.5		–139	0.6	50		–220	2.5	6.5	105	1.0	7.5	1.05
												–89	–90

Note: V_{bkg} was set at –100 mV for pH 7 but was modeled at –90 mV for pH 9. The internal K⁺ concentration was set at 40 mM for all three I/V curves

Table 3 Parameters for modeled currents to fit data from saline APW of pH 9 and 6 (see Fig. 4 and Eqs. 2–5)

pH _o	I _{OH}	I _{irc}					I _{orc}			pH _i	g _{bkg} (S m ⁻²)	E _{OH} (mV)	Resting PD (mV)
		N _{OH} P _{OH} ($\times 10^{-4}$ m s ⁻¹)	V ₅₀₋	z _{g-}	V ₅₀₊	z _{g+}	N _K P _K ($\times 10^{-7}$ m s ⁻¹)	V ₅₀ (mV)	z _g				
9	5.0	–190	0.6	–115	0.6	50	–220	2.8	6.5	32	2.8	7.1	0.5
9	5.0	–180	0.6	–115	0.6			6.5		32	2.8	7.27	0.5
6	14.0	–140	0.8	–50	0.6					7.2	0.85	+81	–51
6	12.0	–145	0.8	–50	0.6			6.5		32	2.8	7.2	0.85
6			50				–198	2.8	6.5	39	2.8		–87

Note. V_{bkg} was set at –90 mV for pH 9 and –88 mV for pH 6

in amplitude as the membrane PD becomes more negative (see Fig. 1d). A similar PD dependence of H⁺/OH[–] channels was calculated from flux measurements in wheat root protoplasts (Tyerman et al. 2001). The half-activation potential, V_{50–} (see Table 1) becomes progressively more negative with time in saline APW. This tendency for H⁺/OH[–] channels to close at PDs more negative than –100 mV in early exposure to saline APW is a probable cause of the membrane PD noise (Al Khazaaly et al. 2009): we postulate that groups of H⁺/OH[–] channels open and close spontaneously as the proton pump still maintains a negative membrane PD. The PD noise is no longer observed once the I/V characteristics indicate that the H⁺/OH[–] state has become dominant. The gating charge z_{g–} remains constant with time in saline APW. The fractional value is taken to indicate partial movement of the charged structural elements of the channel. The low value indicates relatively weak PD dependence.

The resting PD is determined by the balance between the hydroxyl current (Fig. 2d) and the background current (Fig. 2e). Consequently, as the hydroxyl current increases, the membrane PD tends toward E_{OH} (see Table 2). The cytoplasmic pH, pH_i, for *Chara*, *Nitella*, and *Nitellopsis* was found to be in the range of 7.2–7.8 in their native media (Walker and Smith 1975; Smith and Raven 1979; Katsuhara et al. 1989), providing a starting value for pH_i

in the modeling. However, better fits of our data were obtained with pH_i becoming more acidic with time in saline APW (see Table 1). This finding is reasonable, as the presence of the background state maintains the membrane PD negative of E_{OH}, causing outflow of OH[–] out of or inflow of H⁺ into the cytoplasm. This trend is supported by NMR measurements made by Katsuhara et al. (1989), who found that the cytoplasmic pH in *Nitellopsis obtusa* decreased to 6.9 in 2 h of exposure to saline APW.

The inward rectifier channels open at more positive PDs in saline APW (Fig. 2e). A positive shift in half-activation PD was found in the salt-tolerant charophyte *Lamprothamnium* (Al Khazaaly and Beilby, 2007). However, in *Chara* the resting PD is located too far in the positive direction to allow any K⁺ inflow. The [K⁺]_i was set to 40 or 30 mM for modeling I/V characteristics of cells exposed to saline APW for more than 60 min. These values are supported by measurements made by Katsuhara and Tazawa (1986).

The background conductance, which increased by up to an order of magnitude in saline APW, was reduced by the APW wash. The lower background current can be seen as the orange line in Fig. 2e (see also Table 1 for fit parameters). The half-activation potential for the inward rectifier returned to a more negative PD. The I/V curve displayed an unusual shape, with both upward and downward curvature.

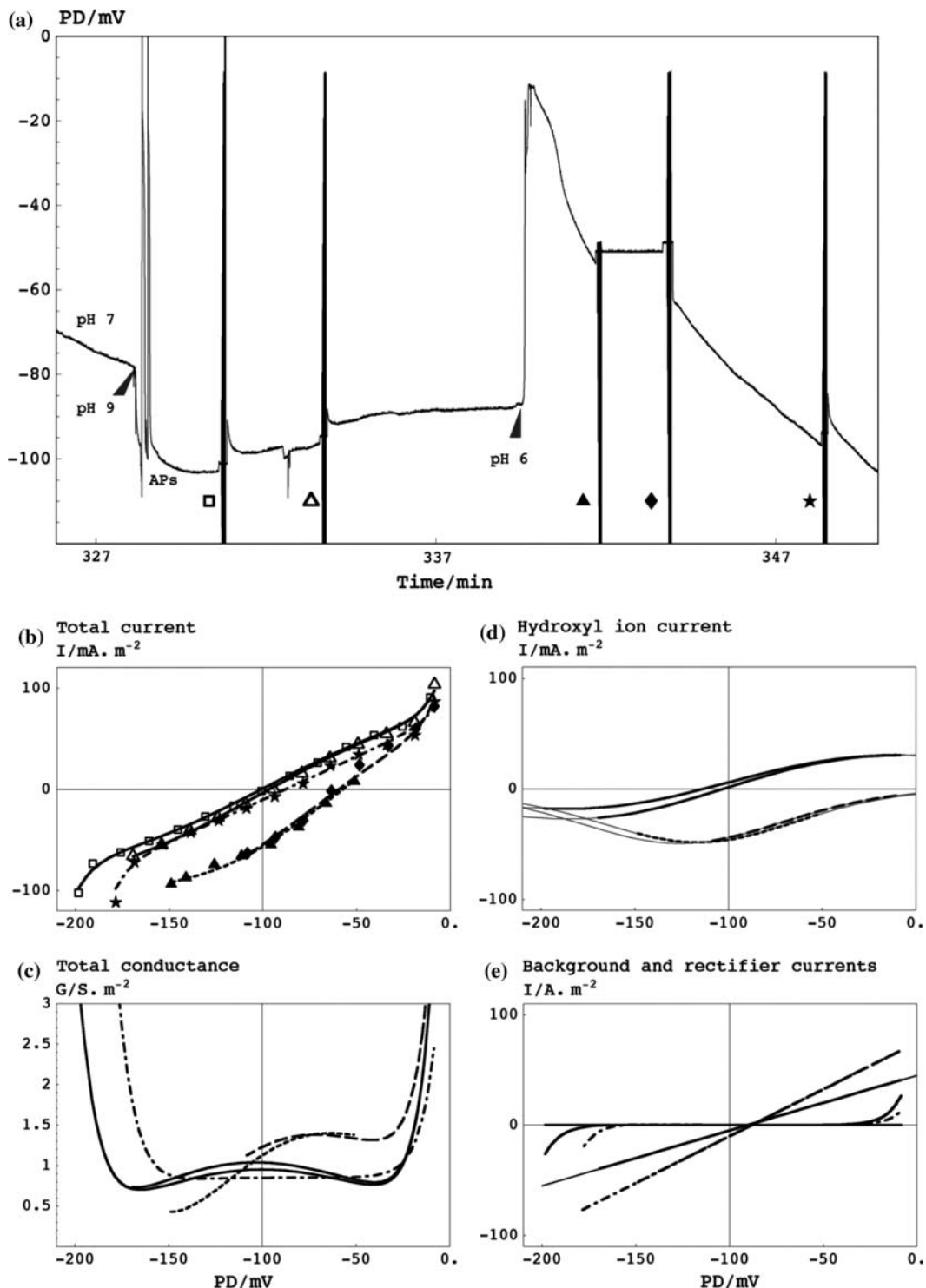


Fig. 4 **a** Response of the membrane PD in saline APW to a change in pH from 7 to 9 and to 6. The membrane PD was data-logged at the faster rate of 10 points/s. The horizontal axis shows the time from the start of the experiment with the cell exposed to saline APW at 136 min. I/V curves appear as vertical lines and are designated by different symbols (open square, open triangle, filled triangle, filled diamond, and star). The changes to pH 9 and pH 6 are indicated by arrows. The membrane PD drift seen before the change to pH 9 is typical of fluctuations observed at this stage of exposure to saline. **b–e** I/V profiles are shown as points using same symbols as in **a**. Modeled

currents are shown by the solid line for pH 9, the short-dashed line for the first I/V curve at pH 6, the long-dashed line for the second I/V curve at pH 6, and the dashed-dotted line for the third I/V curve at pH 6. The membrane PD was clamped at -45 mV between the first two I/Vs at pH 6. The modeling parameters are given in Table 3. **c** G/V profiles obtained by differentiation of the I/V profiles. **d** OH^- currents. The thin solid lines show extrapolation of the model beyond the PD window delimited by the data. **e** Background and rectifier currents. The same types of lines are employed in **b–e**

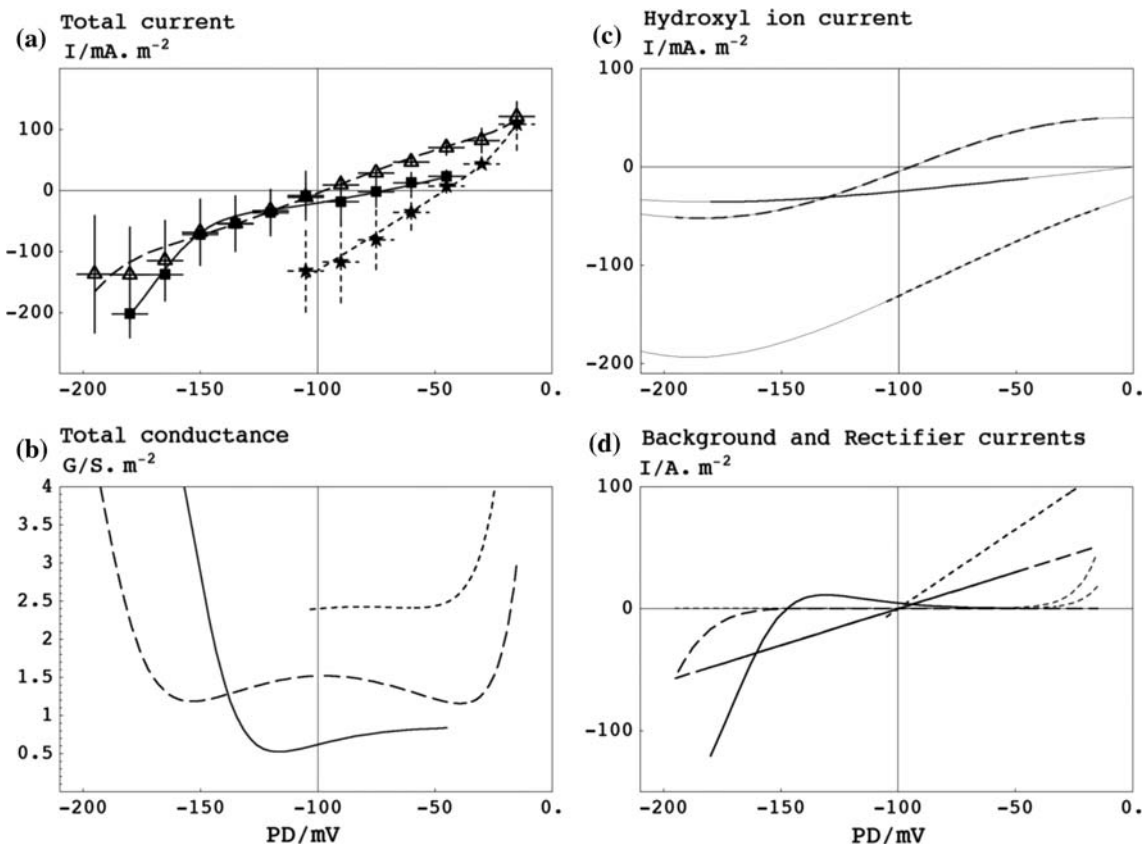


Fig. 5 **a** Statistics of the response of the I/V characteristics in saline APW to pH change. At pH 7, cells 4–8 (four I/V profiles), *filled rectangles*, *solid line*; at pH 9, cells 7 and 8 (four I/V profiles), *open triangles*, *long-dashed line*; at pH 6, cells 7 and 8 (four I/V profiles), *stars*, *short-dashed line*. Data were sorted into 15-mV slots (*horizontal error bars*), with the standard error for each slot given as the *vertical*

error bar. The fitted parameters are given in Table 4. **b** G/V profiles. **c** Fitted OH^- currents. **d** Background and rectifier currents. The line types are the same as in **a–d**. *The thin solid lines* in **d** show extrapolation of the model beyond the PD window delimited by the data

Table 4 Fitted parameters to statistics for the response of I/V characteristics to pH change (see Fig. 5 and Eqs. 2–5)

pH_0	OH^- current				I_{irc}		I_{orc}			pH_1	g_{bkg} (S m^{-2})	E_{OH} (mV)	Resting PD (mV)		
	$N_{\text{OH}}P_{\text{OH}}$ ($\times 10^{-4}$ m s $^{-1}$)	V_{50-}	z_g-	V_{50+}	z_g+	$N_{\text{K}}P_{\text{K}}$ ($\times 10^{-7}$ m s $^{-1}$)	V_{50} (mV)	z_g	$N_{\text{K}}P_{\text{K}}$ ($\times 10^{-7}$ m s $^{-1}$)	V_{50} (mV)	z_g				
7	5.5	–230	0.6			30	–160	2.1				7.1	0.6	0	–70
9	6.0	–200	0.6	–100	0.6	30	–205	2.1	6.5	25	2.8	7.4	0.6	–95	–97
6	45.0	–240	0.6						6.5	20	2.5	6.9	1.3	53	–46

Note: Cells 4–8 (four I/V profiles) at pH 7, cells 4–7 (four I/V profiles) at pH 9, cells 7 and 8 (4 I/V profiles) at pH 6. V_{bkg} was fitted at –100 mV for pH 7, –90 mV for pH 9, and –100 for pH 6. $[\text{K}^+]_i$ was set at 30 mM throughout

This shape can be obtained by a simultaneous fit of both proton pump and hydroxyl channels. The recovery of the proton pumping and gradual closure of the H^+/OH^- channels (see Fig. 2d) suggest that the cell can make a full recovery in APW. This recovery can be slow, as documented for pump recovery from the K^+ state (Beilby 1985).

The pH change experiments support our hypothesis that the H^+/OH^- channels are involved in salinity stress. The membrane PD moved in the right direction in each case. In

medium of pH 7, the E_{OH} was in the range of +30 to 0 mV, depending on the internal pH. In medium of pH 9, the E_{OH} was near –100 mV. In medium of pH 6, the E_{OH} moved to between +50 and +80 mV. The membrane PD settled between E_{OH} and V_{bkg} at pH 9 or 7. At pH 6 there was a positive-going transient and then H^+/OH^- channels closed. The shape of the I/V profiles at pH 9 in Fig. 3 is similar to that observed by Beilby and Bisson (1992). In APW the H^+/OH^- channels close at pH levels < 9 (Beilby and

Bisson 1992), while in saline APW this threshold pH is lowered to values between 7 and 6. It will be interesting to investigate if the lowering of the pH threshold for channel opening depends on the Na^+ concentration of the saline APW.

The Role of H^+/OH^- Channels in Salt Stress in *Chara australis*

Bisson and Walker (1980) found that if the external pH of APW is increased to a threshold value (near pH 9), the surface of the whole cell becomes an alkaline band. Beilby and Bisson (1992) measured the I/V profiles of this high pH state and found that both the conductance and the reversal PD were rather variable. However, the membrane has always reverted to a proton pump-dominated state below pH 9. Thus, finding activation of these channels at pH 7 in saline APW is rather surprising. While the opening of the H^+/OH^- channels in the alkaline band is beneficial for the cell in native pond water, the circumstances are very different under salinity stress. The negative H^+/OH^- current implies outflow of OH^- or inflow of H^+ , acidifying the cytoplasm. The proton pump is inactivated (Shepherd et al. 2008) and the buffering capacity of the cytoplasm is finite. The membrane PD continues to move to more positive levels, reaching the activation threshold for the outward rectifier (about -50 mV), where the cell will lose more K^+ . The balance of K^+ to Na^+ , important for normal metabolism (Maathuis and Amtmann 1999), will be further disrupted. Finally, the increased permeability to H^+/OH^- dissipates some of the proton electrochemical gradient that is needed for $2H^+/Cl^-$ symport and H^+/Na^+ antiport. And, of course, the cell cannot band without the pump to provide the acid regions. The mechanism that increases carbon assimilation is sabotaged. The cell is doomed if it remains in the saline medium. The high Na^+ concentration and Na^+/Ca^{2+} ratio of the medium are clearly the cause of the proton pump inactivation, large background conductance, and H^+/OH^- channel activation, as once the cell is returned to APW, all these effects are gradually reversed (orange curve in Fig. 2b–e).

What happens in salt-tolerant charophytes? Yao and Bisson (1993) found that the alkaline bands in salt-tolerant *Chara buckellii* (*longifolia*) cover more surface area in saline APW than in APW. They observed an increase in membrane conductance and assumed that it is due to activation of H^+/OH^- channels. The key difference from salt-sensitive *Chara australis* is the salinity-activated increase in proton pumping. Thus *Chara longifolia* is able to maintain a negative membrane PD and the banding system. Another salt-tolerant charophyte, *Lamprothamnium*, also exhibits progressively greater membrane conductance as the medium salinity is increased (Beilby and

Shepherd 2001). However, modeling of the I/V characteristics suggests that it is the background conductance that increases (Beilby and Shepherd 2001; Al Khazaaly and Beilby 2007). *Lamprothamnium* has not been observed to band in saline media but does exhibit the high-pH state in alkaline media (Bisson and Kirst 1983). Neither *Chara longifolia* nor *Lamprothamnium* exhibits the sodium-induced noise observed in *Chara australis* (Al Khazaaly et al. 2009).

H^+/OH^- Channels in Roots

Roots of land plants have a system similar to charophyte banding, with proton (or hydroxyl) channels activated at the root tip and proton pumping in the subapical zone of the root (Raven 1991). Wheat root protoplasts were observed to oscillate from a pump-dominated state with H^+ efflux to a state with channel-mediated H^+ influx (Tyerman et al. 2001). If salinity inactivates the pump and opens the proton (or hydroxyl) channels in the subapical zone of roots, this will lead to major disruption of the normal root function (Raven 1991). Tyerman et al. (1997) observed inward currents at membrane PDs more positive than E_K and E_{Cl^-} , as well as salinity-induced noise, in salt-stressed wheat root protoplasts. Consequently, the role of H^+/OH^- channels in salinity stress may extend to many salt-sensitive land plants.

Conclusion

While pH changes can affect various transporters and more experiments are necessary for final identification, we present strong evidence that H^+/OH^- channels open in the latter stages of salinity stress in *Chara australis*. In native pond water these channels are part of the banding mechanism that enhances the cell's carbon assimilation in nonsaline pond media and are closed at pH levels below 9. The activation at neutral pH in saline APW is thus rather unexpected. Under salinity stress the opening of these channels causes a positive-going shift of the membrane PD and possible acidification of the cytoplasm. The electrochemical gradient for H^+ is progressively dissipated, so there is less motive force for H^+/Na^+ antiport and $2H^+/Cl^-$ symport. The membrane PD becomes more positive and outward K^+ rectifier channels are activated, depleting the cell of more K^+ .

References

Al Khazaaly S, Beilby MJ (2007) Modelling ion transporters at the time of hypertonic regulation in *Lamprothamnium succinatum*. Charophytes 1:28–47

Al Khazaaly S, Walker NA, Beilby MJ, Shepherd VA (2009) Membrane potential fluctuations in *Chara australis*: the characteristic signature of high external sodium. *Eur Biophys J* (in press)

Amtmann A, Sanders D (1999) Mechanisms of Na^+ uptake by plant cells. *Adv Bot Res* 29:75–112

Beilby MJ (1984) Current-voltage characteristics of the proton pump at *Chara* plasmalemma. *J Membr Biol* 81:113–125

Beilby MJ (1985) Potassium channels at *Chara* plasmalemma. *J Exp Bot* 36:228–239

Beilby MJ (1986a) Factors controlling the K^+ conductance in *Chara*. *J Membr Biol* 93:187–193

Beilby MJ (1986b) Potassium channels and different states of *Chara* plasmalemma. *J Membr Biol* 89:241–249

Beilby MJ (1989) Electrophysiology of giant algal cells. *Methods Enzymol* 174:403–443

Beilby MJ (1990) Current/voltage curves for plant membrane studies: a critical analysis of the method. *J Exp Bot* 41:165–182

Beilby MJ, Beilby BN (1983) Potential dependence of the admittance of *Chara* plasmalemma. *J Membr Biol* 74:229–245

Beilby MJ, Bisson MA (1992) *Chara* plasmalemma at high pH: voltage dependence of the conductance at rest and during excitation. *J Membr Biol* 125:25–39

Beilby MJ, Shepherd VA (1996) Turgor regulation in *Lamprothamnium papulosum*. I. I/V analysis and pharmacological dissection of the hypotonic effect. *Plant Cell Environ* 19:837–847

Beilby MJ, Shepherd VA (2001) Modeling the current-voltage characteristics of charophyte membranes. II. The effect of salinity on membranes of *Lamprothamnium papulosum*. *J Membr Biol* 181:77–89

Beilby MJ, Shepherd VA (2006) The electrophysiology of salt tolerance in charophytes. *Cryptogamie Algologie* 27:403–417

Beilby MJ, Walker NA (1996) Modeling the current-voltage characteristics of *Chara* membranes: I. The effect of ATP removal and zero turgor. *J Membr Biol* 149:89–101

Bisson MA, Kirst GO (1983) Osmotic adaptations of charophyte algae in the Coorong, South Australia and other Australian lakes. *Hydrobiologia* 105:45–51

Bisson MA, Walker NA (1980) The *Chara* plasmalemma at high pH. Electrical measurements show rapid specific passive uniport of H^+ or OH^- . *J Membr Biol* 56:1–7

Blatt M (1987) Electrical characteristics of stomatal guard cells: the contribution of ATP-dependent, “electrogenic” transport revealed by current-voltage and difference-current–voltage analysis. *J Membr Biol* 98:257–274

Demidchik V, Maathuis FJM (2007) Physiological roles of nonselective cation channels in plants: from stress to signaling and development. *New Phytol* 175:387–404

Demidchik VV, Tester M (2002) Sodium fluxes through nonselective cation channels in plasma membrane of protoplasts from *Arabidopsis* roots. *Plant Physiol* 128:379–387

Demidchik VV, Bowen HC, Maathuis FJM, Shabala SN, Tester M, White PJ, Davies JM (2002) *Arabidopsis thaliana* root nonselective cation channels mediate calcium uptake and are involved in growth. *Plant J* 32:799–808

Garcia A, Chivas AR (2006) Diversity and ecology of extant and Quaternary Australian charophytes (Charales). *Cryptogamie Algologie* 27:323–340

Gradmann D (1989) ATP-driven chloride pump in giant alga *Acetabularia*. *Methods Enzymol* 174:490–504

Hansen U-P, Gradmann D, Sanders D, Slayman CL (1981) Interpretation of current-voltage relationship for “active” ion transport systems: I. steady-state reaction-kinetic analysis of class I mechanisms. *J Membr Biol* 63:165–190

Kamiya N (1959) Protoplasmic streaming. *Protoplasmatologia. Handbuch der Protoplasma-forschung* VIII/3 a. Springer, Wien

Karol KG, McCourt RM, Cimino MT, Delwiche CF (2001) The closest living relatives of land plants. *Science* 294:2351–2353

Katsuhara M, Tazawa M (1986) Salt tolerance in *Nitellopsis obtusa*. *Protoplasma* 135:155–161

Katsuhara M, Kuchitsu K, Takeshige K, Tazawa M (1989) Salt stress-induced cytoplasmic acidification and vacuolar alkalization in *Nitellopsis obtusa* cells. In vivo ^{31}P -nuclear magnetic resonance study. *Plant Physiol* 90:1102–1107

Lucas WJ (1979) Alkaline band formation in *Chara corallina*. Due to OH^- efflux or H^+ influx? *Plant Physiol* 63:248–254

Lucas WJ (1982) Mechanism of acquisition of exogenous bicarbonate by internodal cells of *Chara corallina*. *Planta* 156:181–192

Lucas WJ, Nuccitelli R (1980) HCO_3^- and OH^- transport across the plasmalemma of *Chara corallina*: spatial resolution obtained using extracellular vibrating probe. *Planta* 150:120–131

Lucas WJ, Smith FA (1973) The formation of alkaline and acid regions at the surface of *Chara corallina* cells. *J Exp Bot* 24:1–14

Maathuis FJM, Amtmann A (1999) K^+ nutrition and Na^+ toxicity: the basis of cellular K^+/Na^+ ratios. *Ann Bot* 84:123–133

Prins HBA, Snel JFH, Helder RJ, Zanstra PE (1980) Photosynthetic HCO_3^- utilization and OH^- excretion in aquatic angiosperms. *Plant Physiol* 66:818–822

Raven JA (1991) Terrestrial rhizophytes and H^+ currents circulating over at least a millimeter: an obligate relationship? *New Phytol* 117:177–185

Shepherd VA, Beilby MJ, Heslop D (1999) Ecophysiology of the hypotonic response in the salt-tolerant alga *Lamprothamnium papulosum*. *Plant Cell Environ* 22:333–346

Shepherd VA, Beilby MJ, Shimmen T (2002) Mechanosensory ion channels in charophyte cells: the response to touch and salinity stress. *Eur Biophys J* 31:341–355

Shepherd VA, Beilby MJ, Al Khazaaly S, Shimmen T (2008) Mechano-perception in *Chara* cells: the influence of salinity and calcium on touch-activated receptor potentials, action potentials and ion transport. *Plant Cell Environ* 31:1575–1591

Simons R (1979) Strong electric field effects on transfer between membrane-bound amines and water. *Nature* 280:824–826

Smith FA, Raven JA (1979) Intracellular pH and its regulation. *Ann Rev Plant Physiol* 30:289–311

Smith JR, Walker NA (1983) Membrane conductance of *Chara* measured in the acid and basic zones. *J Membr Biol* 73:193–202

Spear DG, Barr JK, Barr CE (1969) Localization of hydrogen ion and chloride ion fluxes in *Nitella*. *J Gen Physiol* 54:397–414

Tester M (1988a) Pharmacology of K^+ channels in the plasmalemma of the green alga *Chara corallina*. *J Membr Biol* 103:159–169

Tester M (1988b) Blockade of potassium channels in the plasmalemma of *Chara corallina* by tetraethylammonium, Ba^{2+} , Na^+ , and Cs^+ . *J Membr Biol* 105:77–85

Tester M, Davenport R (2003) Na^+ tolerance and Na^+ transport in higher plants. *Ann Bot* 91:503–527

Thiel G, MacRobbie EAC, Blatt MR (1992) Membrane transport in stomatal guard cells: the importance of voltage control. *J Membr Biol* 126:1–18

Tyerman SD, Skerrett M, Garrill A, Findlay GP, Leigh RA (1997) Pathways for the permeation of Na^+ , and Cl^- into protoplasts derived from the cortex of wheat roots. *J Exp Bot* 48:459–480

Tyerman SD, Beilby MJ, Whittington J, Juswono U, Newman I, Shabala S (2001) Oscillations in proton transport revealed from simultaneous measurements of net current and net proton fluxes from isolated root protoplasts: MIFE meets patch-clamp. *Aust J Plant Physiol* 28:591–604

Walker NA (1983) The uptake of inorganic carbon by freshwater plants. *Plant Cell Environ* 6:323–328

Walker NA, Smith FA (1975) Intracellular pH in *Chara corallina* measured by DMO distribution. *Plant Sci Lett* 4:125–132

Walker NA, Smith FA (1977) Circulating electric currents between acid and alkaline zones associated with HCO_3^- assimilation in *Chara*. *J Exp Bot* 28:1190–1206

Walker NA, Smith FA, Cathers IR (1980) Bicarbonate assimilation by freshwater charophytes and higher plants: I. membrane transport of bicarbonate ions is not proven. *J Membr Biol* 57:51–58

Yao X, Bisson MA (1993) Passive proton conductance is the major reason for membrane depolarization and conductance increase in *Chara buckellii* in high-salt conditions. *Plant Physiol* 103:197–203

Yao X, Bisson MA, Brzezicki LJ (1992) ATP-driven proton pumping in two species of *Chara* differing in salt tolerance. *Plant Cell Environ* 15:199–210